

Local rotational symmetry effects on Fano resonances with constant non-resonant transmission channel

Bo-Hong Li, Houfang Liu, Fei Cheng, Jing Han, Hong Xiao et al.

Citation: *Appl. Phys. Lett.* **101**, 031114 (2012); doi: 10.1063/1.4737178

View online: <http://dx.doi.org/10.1063/1.4737178>

View Table of Contents: <http://apl.aip.org/resource/1/APPLAB/v101/i3>

Published by the [American Institute of Physics](http://www.aip.org).

Related Articles

Tuning the wavelength of amplified spontaneous emission coupled to localized surface plasmon
Appl. Phys. Lett. **101**, 031117 (2012)

Plasmonic mediated nucleation of resonant nano-cavities
Appl. Phys. Lett. **101**, 031911 (2012)

Interparticle coupling of plasmon fields due to reorganization of Au nanoparticles in Langmuir-Blodgett film
J. Appl. Phys. **112**, 014323 (2012)

Measuring optical phonon dynamics in a bismuth thin film through a surface plasmon resonance
J. Appl. Phys. **112**, 013527 (2012)

Surface-bound-exciton emission associated with domain interfaces in m-plane ZnO films
Appl. Phys. Lett. **101**, 011901 (2012)

Additional information on *Appl. Phys. Lett.*

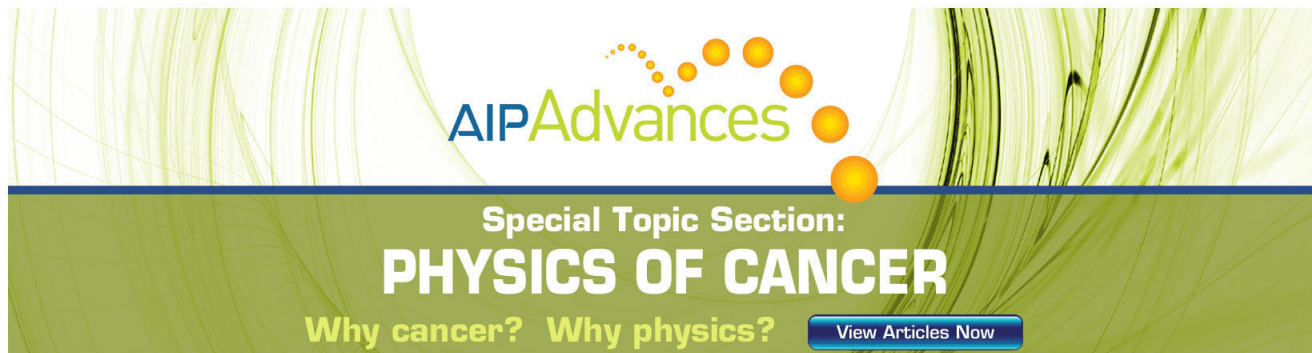
Journal Homepage: <http://apl.aip.org/>

Journal Information: http://apl.aip.org/about/about_the_journal

Top downloads: http://apl.aip.org/features/most_downloaded

Information for Authors: <http://apl.aip.org/authors>

ADVERTISEMENT



AIPAdvances

Special Topic Section:
PHYSICS OF CANCER

Why cancer? Why physics? [View Articles Now](#)

Local rotational symmetry effects on Fano resonances with constant non-resonant transmission channel

Bo-Hong Li (李博宏), Houfang Liu (刘厚方), Fei Cheng (程飞), Jing Han (韩静), Hong Xiao (肖宏), Xiufeng Han (韩秀峰), Changzhi Gu (顾长志), and Xiangqiang Qiu (邱祥冈)^{a)}

Beijing National Laboratory for Condensed Matter Physics and Institute of Physics, Chinese Academy of Sciences, Beijing 100190, China

(Received 6 June 2012; accepted 28 June 2012; published online 19 July 2012)

Three kinds of 12-fold quasi-periodic subwavelength hole arrays have been designed using the same dodecahedral supercell arranged with different local rotational symmetries. Fano resonances associated with spoof surface plasmons in these structures have been studied by far-infrared transmission measurements. The resonant transmission channels of the lowest-order Fano resonance mode have been compared directly between these structures, benefitting from constant non-resonant transmission channel. It is found that the higher is the local rotational symmetry of the supercell array, the higher the transmission intensity and the narrower the linewidth of the Fano resonance. © 2012 American Institute of Physics. [<http://dx.doi.org/10.1063/1.4737178>]

Fano resonances¹ in plasmonics have attracted much interest because of its underlying physics and potential applications.^{2–5} For extraordinary optical transmission (EOT) through two-dimensional subwavelength hole arrays in metal films,⁶ Fano resonances can be identified by their far-field response, which is characterized by an asymmetric lineshape, resulting from the coupling between the non-resonant transmission channel through isolated holes and the resonant transmission channel mediated by surface plasmon polaritons (SPPs).⁷ Due to the important role played by the hole array in SPP excitation, intensive efforts have been devoted to investigating the effects of the geometric configuration of the hole array on the resonant transmission channel of Fano resonances in EOT.^{8–14} However, it is a challenge to compare the resonant transmission channels directly between different geometric configurations while keeping both the non-resonant transmission channel and the Fano resonance peak wavelength unchanged. We also notice that previous research on Fano resonances in EOT mainly focuses on the visible^{7,15} and terahertz^{11,16} regimes. However, the infrared regime holds significant promise on bio-sensing,^{17,18} imaging,^{19,20} and integrating electronic with plasmonic devices and provides convenience of structure fabrication,²¹ so it is of great interest to study Fano resonances in EOT in this spectral region.

We have designed three kinds of quasi-periodic structures consisting of identical dodecahedral supercells placed at the vertices of hexagonal (pattern I), square (pattern II), and Stampfli²² (pattern III) parent lattices (Figs. 1(a)–1(c)). The hole diameter d , the density of holes ρ , the distance between the nearest-neighbour holes a and the local rotational symmetry order of the hole array n are the same for all three structures. Meanwhile, the ratio of d to a is properly chosen, so that the lowest-order Fano resonance mode is strengthened and other modes are suppressed,¹¹ providing convenience of Fano lineshape analysis.^{7,15,16,23} Then, the influence of the local rotational symmetry of the supercell

array on the resonant transmission channel of the Fano resonance was explored by EOT spectra measurements in the far-infrared (FIR) regime, where the resonant transmission channel is assisted by spoof surface plasmons (SSPs),²⁴ instead of SPPs. We find that the structure with higher-order local rotational symmetry of the supercell array has higher transmission intensity and narrower linewidth of the Fano resonance.

A 5-nm-thick Ta adhesion layer and a 100-nm-thick Au film were successively deposited on a 450- μm -thick Si substrate by magnetron sputtering. Subwavelength hole arrays were fabricated in metal films using ultraviolet photolithography and reactive ion etching, with each hole array occupying an area of about $7 \times 7 \text{ mm}^2$. All the structures mentioned in this Letter have $d = 4 \mu\text{m}$ and $a = 10 \mu\text{m}$. For the three quasi-periodic structures (Figs. 1(a)–1(c)), the distance between the nearest-neighbor supercells $A = \tau a$, where $\tau = 2 + \sqrt{3}$ is Dodecanacci number. Shown in Figs. 1(d)–1(f) are scanning electron microscopy (SEM) images of the three structures. Figs. 1(g)–1(i) show their corresponding reciprocal spaces obtained by two-dimensional fast Fourier transform (2D-FFT) calculations. Well-defined local 12-fold rotational symmetry of the hole array can be clearly seen, resulting from the same dodecahedral supercell, in which separation angles around each hole are multiples of 30° .²⁵ The dodecahedral Brillouin zone defined by the innermost 12 bright spots in the reciprocal space owns a reciprocal vector close to $2\pi/a$.^{11,26} Around these main spots, the satellite ones with much weaker brightness are associated with the reciprocal vectors of the parent lattices.

Normal incident relative transmission spectra $T_R(\lambda) = T_{Au}(\lambda)/T_{Si}(\lambda)$ in the FIR regime were obtained using a Fourier transform infrared spectrometer (DA8, Bomem Inc.), where $T_{Au}(\lambda)$ and $T_{Si}(\lambda)$ are the transmission spectra of the perforated Au film on Si substrate and a bare Si substrate, respectively. Shown in Fig. 2(a) are the normalized transmission spectra $T_N(\lambda) = T_R(\lambda)/f$, where f is the fractional hole area, i.e., the filling factor. The transmission spectra exhibit obvious EOT resonant behaviors.¹¹ The lowest-order Fano

^{a)}Electronic mail: xgqiu@iphy.ac.cn.

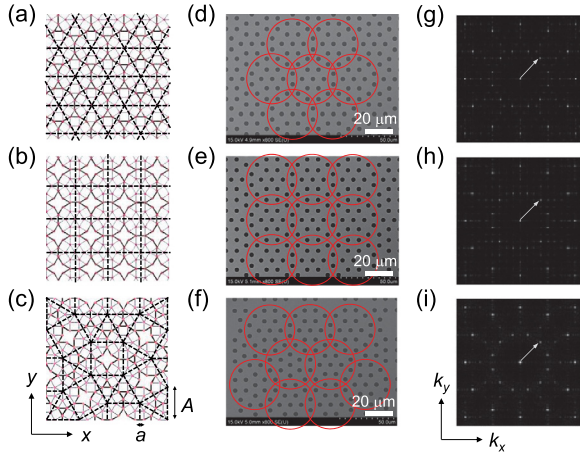


FIG. 1. Real and reciprocal spaces of structures. (a)–(c), Schematics of patterns I, II, and III with the hexagonal (a), square (b), and Stampfli (c) parent lattices (indicated by black thick lines), respectively. In all three structures, the same dodecahedral supercell as the “unit cell” locates at each vertex of the parent lattices. a and $A (=a(2 + \sqrt{3}))$ is the distance between the nearest-neighbour holes and supercells, respectively. (d)–(f) Corresponding SEM images of structures in (a)–(c). Red circles are guides for the eye, referring to supercells. (g)–(i) Reciprocal spaces of the three structures in (a)–(c) by 2D-FFT calculations. The reciprocal vector indicated by the white arrow is close to $2\pi/a$.

resonance peak Q_1 locates at nearly the same wavelength for the three structures. For comparison, the transmission spectra of simple hexagonal ($n=6$) and simple square ($n=4$) arrays of holes were also measured (data not shown here) and the positions of their lowest-order Fano resonance peaks H_1 and S_1 are indicated in Fig. 2(a). It is obvious that in spite of the same a and d , the simple hexagonal, simple square, and 12-fold quasi-periodic lattices show different wavelengths of the lowest-order Fano resonance peak ($H_1 < Q_1 < S_1$), due to different local rotational symmetries of the hole array.

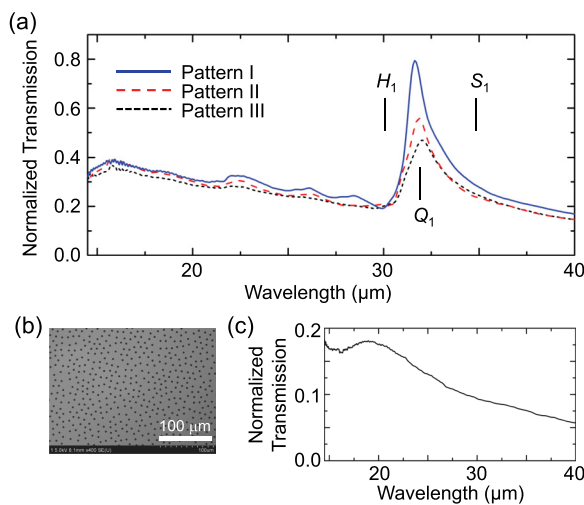


FIG. 2. Experimental transmission spectra. (a) Experimental normal incident transmission spectra of patterns I (blue), II (red), and III (black), respectively, in the FIR regime. The lowest-order Fano resonance peaks (vertical lines) are indicated for simple hexagonal (H_1), simple square (S_1), and quasi-periodic (Q_1) lattices, respectively. (b) SEM image of a randomly distributed hole array in Au film. (c) Experimental normal incident transmission spectrum of the structure in (b) in the FIR regime.

As shown in Fig. 2(a), the transmission spectra of all three structures are dominated by the lowest-order SSP mode, which exhibits typical Fano lineshape. In these three structures, d and ρ are equal, leading to an identical filling factor of 13.54% in our case. Thus, the non-resonant transmission channel can be considered identical for these structures. As a result, the transmission spectra of all three structures are superposed on the same background (Fig. 2(a)). Since the non-resonant transmission channel and the lowest-order Fano resonance peak wavelength remain unchanged, the effects of the geometric configuration on the resonant transmission channels can, therefore, be explored. In order to make a quantitative comparison, the experimental transmission spectra are fitted using the Fano resonance model.^{1,7} The total transmission $T(\lambda)$ of the Fano resonance peak can be described as

$$T(\lambda) = T_B(\lambda) + C \frac{(\lambda - \lambda_R + q\Gamma/2)^2}{(\lambda - \lambda_R)^2 + (\Gamma/2)^2}, \quad (1)$$

where $T_B(\lambda)$ is the background transmission following Bethe theory,²⁷ C is the non-resonant transmission coefficient, λ is the wavelength of incident light, λ_R is the resonant wavelength, q is the asymmetry parameter of the profile, and Γ is the linewidth of the Fano resonance peak, which characterizes the damping of SSPs. In order to obtain $T_B(\lambda)$, we fabricated another Au film patterned with randomly distributed holes (Fig. 2(b)). The transmission spectrum of this sample was measured (Fig. 2(c)) and used as $T_B(\lambda)$ in Eq. (1).^{11,28,29} Since $\lambda_R = \lambda_P - \Gamma/2q$ and $C = F_P/(1 + q^2)$ can be deduced from $\partial F(\lambda = \lambda_P)/\partial \lambda = 0$ and $F_P \equiv T(\lambda_P) - T(\lambda_V)$, respectively, Eq. (1) can be reduced to

$$F(\lambda) \equiv T(\lambda) - T_B(\lambda) = \frac{F_P}{(1 + q^2)} \frac{[\lambda - \lambda_P + (q + 1/q)\Gamma/2]^2}{(\lambda - \lambda_P + \Gamma/2q)^2 + (\Gamma/2)^2}, \quad (2)$$

where F_P is the difference of the transmission intensity between the Fano resonance peak and valley, and λ_P (λ_V) is the Fano resonance peak (valley) wavelength. Since both F_P and λ_P can be obtained directly from experimental transmission spectra, only two fitting parameters, q and Γ , remains in Eq. (2). The fitted transmission spectra are

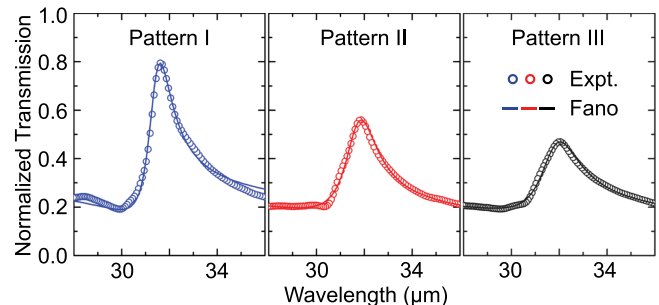


FIG. 3. Experimental and fitted transmission spectra. Experimental normal incident transmission spectra (hollow circles) around the lowest-order Fano resonance mode and their Fano lineshape fitting results (solid lines) for patterns I (blue), II (red), and III (black).

TABLE I. Characteristic parameters of the lowest-order resonant peak.

Pattern	λ_P^a	T_N	Γ^a	Q	L_{SSP}^a	L_{SSP}/A
I	31.6	0.794	1.16	27.2	40.0	1.07
II	31.9	0.560	1.62	19.6	29.1	0.78
III	32.1	0.469	1.96	16.2	24.1	0.65

^aunit: μm .

plotted in Fig. 3 and the corresponding parameters are summarized in Table I.

For the lowest-order Fano resonance mode, pattern I exhibits the highest transmission intensity, followed by pattern II, then pattern III. Meanwhile, the linewidth Γ of pattern I is the narrowest among these structures, followed by pattern II, then Pattern III. Since the non-resonant transmission channel of the Fano resonance is identical for all three structures, we conclude that pattern I has the strongest resonant transmission channel. Correspondingly, the quality factor $Q = \lambda_R/\Gamma$ follows pattern I>II>III. The difference is due to different local rotational symmetries of the supercell array of these three structures. When the incident light impinges on the film, it is scattered by the hole array, exciting SSPs. SSPs propagate along the interface and their interference assists the resonant transmission channel. However, SSPs suffer losses from the scattering by the holes, surface roughness, and grain boundaries,^{30,31} so not all the holes contribute to the resonant transmission channel but mainly those within the span of the SSPs' propagation length L_{SSP} .^{32,33} This characteristic length can be evaluated as $L_{SSP} = \lambda_R^2/(2\pi n_{eff} \Gamma)$,²⁹ where the effective refraction index $n_{eff} = \sqrt{\epsilon_m \epsilon_d / (\epsilon_m + \epsilon_d)}$ with ϵ_m ($\sim \infty$ for Au in the FIR regime) and ϵ_d (11.9 for Si in the FIR regime) the respective dielectric constants of the metal and the dielectric. As listed in Table I, L_{SSP} in all three structures is comparable with A . In other words, the resonant transmission channel is mainly influenced by the local geometric configuration of adjacent supercells. The supercell array in pattern I has a local 6-fold rotational symmetry, which is higher than the local 4-fold rotational symmetry of the supercell array in pattern II, resulting in stronger constructive interference of SSPs in pattern I than in pattern II. As for pattern III, though there are five nearest neighbors for each supercell, there is no local rotational symmetry of the supercell array, leading to the weakest constructive interference of SSPs. Consequently, pattern III exhibits the lowest transmission intensity and the broadest linewidth among three structures. Therefore, for different structures with identical local rotational symmetry of the hole array, higher local rotational symmetry of the supercell array leads to stronger constructive interference of SSPs and, consequently, the higher transmission intensity and narrower linewidth of the Fano resonance.

In conclusion, three 12-fold quasi-periodic structures characterized by an identical supercell have been designed with different geometric configurations and their normal incident transmission spectra in the FIR regime have been measured. Constant non-resonant transmission channel in these structures has been realized and resonant transmission channels have been compared through Fano lineshape analysis. The lowest-order Fano resonance peak wavelength is

governed by both the distance between the nearest-neighbour holes and the local rotational symmetry of the hole array. More importantly, structures with higher local rotational symmetry of the supercell array are found to have higher transmission intensity and narrower linewidth of the Fano resonance. Therefore, the resonant transmission channel of the Fano resonance involving SSPs can be tailored by changing the rotational symmetry of the supercell array, while both the non-resonant transmission channel and the Fano resonance peak wavelength stay the same. Furthermore, although experimental results presented here are in the FIR regime, our discussions can also be extended down to the visible and up to THz regimes. We expect our methods of designing structures and analyzing spectra are useful not only to reveal underlying physics of Fano resonances in EOT but also to develop functional plasmonic devices.

We thank Zhiyuan Li, Institute of Physics, Chinese Academy of Sciences and Charlotte E. Sanders, Department of Physics, University of Texas at Austin for discussions. This work is supported by National Basic Research Program of China (Nos. 2009CB929102, 2011CBA00107, and 2012CB921302), National Science Foundation of China (Nos. 10974241, 11104335, and 91121004), and the Knowledge Innovation Program of CAS (No. KJCX2-EW-W02).

¹U. Fano, *Phys. Rev.* **124**, 1866 (1961).²A. E. Miroshnichenko, S. Flach, and Y. S. Kivshar, *Rev. Mod. Phys.* **82**, 2257 (2010).³B. Luk'yanchuk, N. I. Zheludev, S. A. Maier, N. J. Halas, P. Nordlander, H. Giessen, and C. T. Chong, *Nature Mater.* **9**, 707 (2010).⁴V. Giannini, Y. Francescato, H. Amrania, C. C. Phillips, and S. A. Maier, *Nano Lett.* **11**, 2835 (2011).⁵B. Gallinet and O. J. F. Martin, *Phys. Rev. B* **83**, 235427 (2011).⁶T. W. Ebbesen, H. J. Lezec, H. F. Ghaemi, T. Thio, and P. A. Wolff, *Nature (London)* **391**, 667 (1998).⁷C. Genet, M. P. van Exter, and J. P. Woerdman, *Opt. Commun.* **225**, 331 (2003).⁸Q.-J. Wang, J.-Q. Li, C.-P. Huang, C. Zhang, and Y.-Y. Zhu, *Appl. Phys. Lett.* **87**, 091105 (2005).⁹M. Sun, J. Tian, S. Han, Z. Li, B. Cheng, D. Zhang, A. Jin, and H. Yang, *J. Appl. Phys.* **100**, 024320 (2006).¹⁰J. Bravo-Abad, A. I. Fernández-Domínguez, F. J. García-Vidal, and L. Martín-Moreno, *Phys. Rev. Lett.* **99**, 203905 (2007).¹¹T. Matsui, A. Agrawal, A. Nahata, and Z. V. Vardeny, *Nature (London)* **446**, 517 (2007).¹²D. Pacifici, H. J. Lezec, L. A. Sweatlock, R. J. Walters, and H. A. Atwater, *Opt. Express* **16**, 9222 (2008).¹³J. Xue, B.-Q. Dong, X. Wang, R. Yang, Z.-C. Xu, Y. Chen, E. Huq, W. Zeng, X.-P. Qu, and R. Liu, *Microelectron. Eng.* **87**, 1340 (2010).¹⁴H. E. Arabi, M. Park, M. Pourmourey, and K. Oh, *Opt. Express* **19**, 8514 (2011).¹⁵S.-H. Chang, S. Gray, and G. Schatz, *Opt. Express* **13**, 3150 (2005).¹⁶W. Zhang, *Eur. Phys. J. Appl. Phys.* **43**, 1 (2008).¹⁷C.-Y. Chao and L. J. Guo, *Appl. Phys. Lett.* **83**, 1527 (2003).¹⁸R. Adato, A. A. Yanik, J. J. Amsden, D. L. Kaplan, F. G. Omenetto, M. K. Hong, S. Erramilli, and H. Altug, *Proc. Natl. Acad. Sci. U.S.A.* **106**, 19227 (2009).¹⁹M. Schnell, P. Alonso-Gonzalez, L. Arzubia, F. Casanova, L. E. Hueso, A. Chuvilin, and R. Hillenbrand, *Nature Photon.* **5**, 283 (2011).²⁰S. J. Lee, Z. Ku, A. Barve, J. Montoya, W.-Y. Jang, S. R. J. Brueck, M. Sundaram, A. Reisinger, S. Krishna, and S. K. Noh, *Nature Commun.* **2**, 286 (2011).²¹Y.-H. Ye and J.-Y. Zhang, *Appl. Phys. Lett.* **84**, 2977 (2004).²²P. Stampfli, *Helv. Phys. Acta* **59**, 1260 (1986).²³W. Fan, S. Zhang, B. Minhas, K. J. Malloy, and S. R. J. Brueck, *Phys. Rev. Lett.* **94**, 033902 (2005).²⁴J. B. Pendry, L. Martín-Moreno, and F. J. García-Vidal, *Science* **305**, 847 (2004).

- ²⁵S. David, A. Chelnokov, and J.-M. Lourtioz, *Opt. Lett.* **25**, 1001 (2000).
- ²⁶M. E. Zoorob, M. D. B. Charlton, G. J. Parker, J. J. Baumberg, and M. C. Netti, *Nature (London)* **404**, 740 (2000).
- ²⁷H. A. Bethe, *Phys. Rev.* **66**, 163 (1944).
- ²⁸F. van Beijnum, C. Rétif, C. B. Smiet, and M. P. van Exter, *Opt. Lett.* **36**, 3666 (2011).
- ²⁹F. Przybilla, C. Genet, and T. W. Ebbesen, *Opt. Express* **20**, 4697 (2012).
- ³⁰D. S. Kim, S. C. Hohng, V. Malyarchuk, Y. C. Yoon, Y. H. Ahn, K. J. Yee, J. W. Park, J. Kim, Q. H. Park, and C. Lienau, *Phys. Rev. Lett.* **91**, 143901 (2003).
- ³¹M. Kuttge, E. J. R. Vesseur, J. Verhoeven, H. J. Lezec, H. A. Atwater, and A. Polman, *Appl. Phys. Lett.* **93**, 113110 (2008).
- ³²F. Przybilla, C. Genet, and T. W. Ebbesen, *Appl. Phys. Lett.* **89**, 121115 (2006).
- ³³F. Przybilla, A. Degiron, C. Genet, T. Ebbesen, F. de León-Pérez, J. Bravo-Abad, F. J. García-Vidal, and L. Martín-Moreno, *Opt. Express* **16**, 9571 (2008).